

## Spectral $\rho Z$ -Projection Method for Characterization of Body Fluids in Computed Tomography: Ex Vivo Experiments<sup>1</sup>

Andreas H. Mahnken, MD, MBA, Sven Stanzel, MSc, Bjoern Heismann, PhD

**Rationale and Objectives.** The identification of body fluids in computed tomography poses a major diagnostic challenge. The chemical composition of body fluids deviates only slightly from water with very similar computed tomographic (CT) values, which typically range from 0 to 100 HU. The aim of this study was to assess physical and chemical properties of different body fluids in an ex vivo setting.

**Materials and Methods.** A total of 44 samples of blood, blood mixed with pus, pus, bile, and urine obtained during diagnostic and therapeutic punctures were scanned at 80 and 140 kV. Data was quantitatively assessed using the spectral  $\rho Z$ -projection algorithm, which converts dual-energy CT scans into mass density ( $\rho$ ) and effective atomic number ( $Z_{eff}$ ) information.

**Results.** Attenuation values measured at 80 and 140 kV were largely overlapping. CT values allowed, to some degree, for the differentiation of bile or pus from blood or the blood/pus mixture. By applying the  $\rho Z$ -projection, most substances, except for urine, were distinguishable with only small standard deviations ranging between 0.003 and 0.007 g/cm<sup>3</sup> for mass density and between 0.020 and 0.043 for  $Z_{eff}$ .

**Conclusion.** The  $\rho Z$ -projection method is suited to quantitatively assess mass density and effective atomic number of ex vivo body fluid samples. In clinical routine, this technique might be useful for identifying unclear fluid collections even in unenhanced computed tomography.

**Key Words.** Dual energy; computed tomography; material decomposition; spectral computed tomography.

© AUR, 2009

Computed tomography is one of the most important non-invasive diagnostic imaging modalities. It provides three-dimensional representations of the x-ray attenuation coefficient  $\mu(r)$  with submillimeter spatial resolution. However, it is limited in soft tissue contrast resolution (1). Various types of soft tissue and lesions differ only slightly in density and chemical composition and thus their measured x-ray attenuation coefficients are very similar.

To overcome this limitation, intravenous contrast agents are routinely administered. However, differentiation of non-perfused fluid collections such as hematoma, lymphoceles, abscess, or urinoma remains difficult (2), particularly if there are ambiguous clinical findings, or shortly after surgery. Moreover, there are many patients who may not receive iodinated contrast agents. Over the last decade, several studies have addressed the problem of fluid differentiation in computed tomography, but failed to provide clinically applicable solutions (1,3). Thus, low contrast resolution of noncontrast enhanced computed tomography is still a relevant issue in fluid differentiation.

As early as 1976, dual-energy methods were suggested for enhancing the soft tissue contrast in computed tomography (4,5). With the introduction of dual source computed tomographic (CT) dual-energy, imaging became available for clinical routine use. Commercially available dual-energy imaging algorithms are based on a modification of the

Acad Radiol 2009; 16:763-769

<sup>1</sup> From the Department of Diagnostic Radiology and Applied Medical Engineering, Helmholtz Institute (A.H.M.) and Institute of Medical Statistics (S.S.), RWTH Aachen University, Pauwelsstrasse 30, D 52074, Aachen, Germany; and Siemens Healthcare, Forchheim, Germany (B.H.). Received November 19, 2008; accepted January 2, 2009. **Address correspondence to:** A.H.M. e-mail: mahnken@rad.rwth-aachen.de

© AUR, 2009

doi:10.1016/j.acra.2009.01.002

two-material decomposition. This technique is particularly suited for differentiating substances with high atomic numbers such as calcium and iodine. However, other techniques like the  $\rho Z$ -projection, are available (6). The latter converts dual-energy data to mass density and effective atomic number information. In the  $\rho Z$ -projection, the mass density ( $\rho$ ) and the effective atomic number ( $Z_{\text{eff}}$ ) of the absorber completely determine the measured attenuation coefficient for given spectral source  $S(E)$  and detector characteristics  $D(E)$ . Thus,  $Z_{\text{eff}}$  describes the chemical classification and  $\rho$  the physical Morphology of the absorbing material. Converting dual-energy data to mass density and effective atomic number is used for detecting explosives in luggage control, but is not yet established for diagnostic purposes in medicine.

The aim of this study was to establish the medical use of this dual-energy technique by quantitatively characterizing different body fluids in an ex vivo setting using an experimental implementation of the  $\rho Z$ -projection algorithm.

## MATERIAL AND METHODS

Forty-four samples of body fluids from diagnostic and therapeutic punctures were collected after informed consent of the adult patients was obtained. The specimens comprise blood ( $n = 10$ ), bile ( $n = 13$ ), pus ( $n = 5$ ), urine ( $n = 7$ ), as well as a mixture of blood and pus ( $n = 9$ ). All except the urine sample were placed in sterile plastic syringes with a diameter of 1 cm. Urine was placed in slightly bigger plastic containers. All examinations were performed under a waiver from the local ethics committee.

Immediately after the probe sampling was finished, the fluids were examined using a 4-slice CT scanner (SOMATOM Sensation 4; Siemens Medical Solutions, Forchheim, Germany). For CT scanning, the samples were positioned at the isocenter of the scanner gantry. Two sequential image acquisitions were performed at a fixed table position. A  $4 \times 1$  mm collimation and a gantry rotation time of 1 second were applied. The first scan was performed at a tube voltage ( $U_1$ ) of 80 kV with 0.6 mm titanium (Ti) pre-filtering and a tube current-time product of 300 mAs. The second scan was performed at a tube voltage ( $U_2$ ) of 140 kV with 1.2 mm Ti pre-filtering and a tube current-time product of 300 mAs (Fig 1).

For image reconstruction, a slice width of 1 mm and a sharp convolution kernel (B80s) were chosen with a field of view of  $200 \times 200$  mm<sup>2</sup> and a  $512 \times 512$  matrix.

The corresponding reconstructed CT images of the 80 and 140 kV measurements were transferred to a separate computer equipped with a dedicated MatLab (Mathworks, Natick, MA) based software tool for performing the  $\rho Z$ -projection (6). A summary of the  $\rho Z$ -projection is described in the Appendix. Thereafter, the results of the

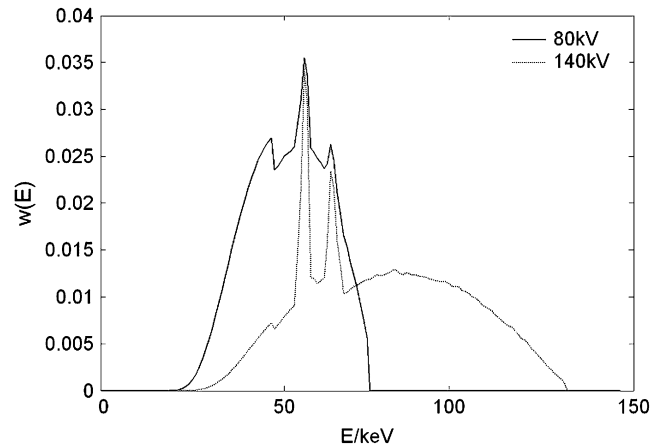


**Figure 1.** The source spectra  $S_{1,2}(E)$  as they were used in this experiment. At 80 kV a 0.6 mm titanium pre-filtering was used, whereas 1.2 mm titanium pre-filtering was applied at a tube voltage of 140 kV.

$\rho Z$ -projection were transcribed into separate stack of DICOM images bearing either the mass density ( $\rho$ ) or the effective atomic number ( $Z_{\text{eff}}$ ). The  $\rho Z$ -projection images were transferred to the CT scanner and used as input for further evaluation (Fig 2). For quantitative assessment, a representative section was selected from the center of each sample and a region-of-interest of 150 to 200 voxels was selected from four subsequent slices. The mean value of these regions-of-interest was taken for analysis.

To confirm the composition of the specimen (blood, pus, mixture of blood and pus) or to exclude contamination with blood after a diagnostic or therapeutic puncture (bile, urine), all samples were analyzed microscopically after the CT scan.

For further analysis, data were summarized by minimum, maximum, mean, and corresponding standard deviation. Attenuation values at 80 and 140 kV, mass density, and effective atomic number were graphically displayed. Multiple *t*-tests were performed for comparing the means of the different categories of fluids for each imaging parameter (80 kV, 140 kV,  $\rho$ ,  $Z_{\text{eff}}$ ). A *P* value of  $< .05$  was considered statistically significant. As this is an explorative study, no  $\alpha$ -adjustment was performed.

## RESULTS

All samples were scanned between 1 to 9 minutes after sampling. There were no problems during data acquisition. One sample of blood had to be excluded from further analysis due to macroscopically visible clotting (Fig 2).

In general, the attenuation values show a wide overlap for both tube voltages and most of the sample types (Fig 3). Bile and pus can be separated from blood and the blood/pus

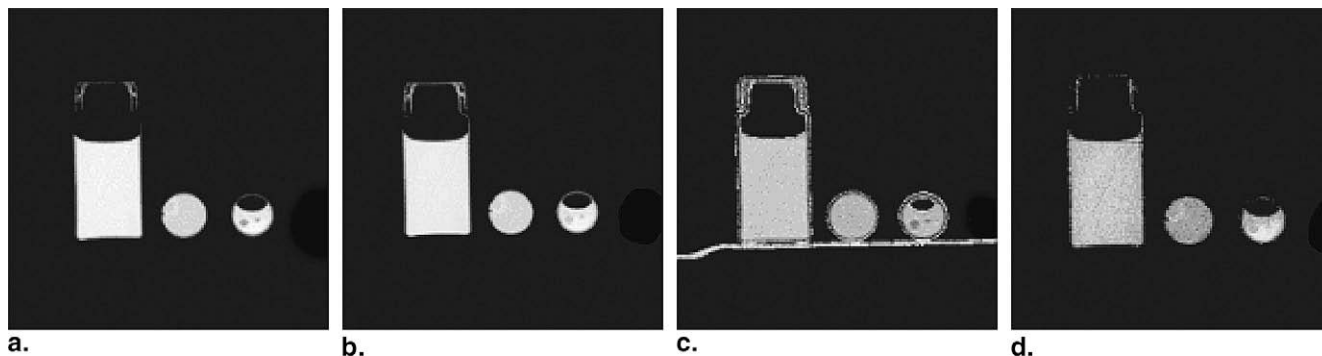


**Figure 2.** Attenuation images of a dual sequence computed tomographic scan with 80 kV (a) and 140 kV tube voltage (b) show a container with urine and syringes filled with water and blood. The gray scale window settings were: center = 100 HU, width = 400 HU. The corresponding  $Z$  images (c) were centered at 7.0 with a width of 5.0. The corresponding  $\rho$  image (d) is displayed with a center of  $1.0 \text{ g/cm}^3$  and a width of  $0.2 \text{ g/cm}^3$ . Note the heterogeneous appearance of the blood sample, which is due to clotting. Subsequently this sample was excluded from analysis.

mixture, whereas the other samples exhibit relevant overlaps. In particular, the urine sample values are widely spread.

The  $\rho Z$  values show a clustering with low standard deviations for all substances except for urine (Table 1, Fig 4). The standard deviations for mass density range from  $0.003 \text{ g/cm}^3$  for the samples of pus to  $0.011 \text{ g/cm}^3$  for the urine samples. For  $Z_{\text{eff}}$ , the standard deviation ranges from 0.020 for the samples of blood to 0.149 for the urine samples.

Apart from urine, the most samples can be separated. Compared to the attenuation values at 80 and 140 kV, separation of blood from mixtures of blood and pus became feasible with the  $\rho Z$  projection method. The samples of pus have a higher effective atomic number than blood, whereas this is reversed for the mass density. The samples of the blood and pus mixture consequently take up intermediate values. This is confirmed by statistical analysis. Applying the  $\rho Z$ -projection method, there are significant differences comparing blood with mixtures from blood and pus, whereas there are no significant differences when using attenuation values at 80 and 140 kV for differentiating blood from mixtures of blood and pus (Table 2).

## DISCUSSION

As early as 1976, a dual-energy CT method was proposed to improve contrast resolution (4,5). The basic idea of the basis material decomposition was to independently determine the coefficients of photoelectric absorption and Compton scatter attenuation by two CT measurements with different tube voltages. Alternate sets of basis functions, e.g., the attenuation functions of water and bone material, were applied. Several technical and clinical studies investigated the use of this technique (7–10). The latter was implemented into a commercially available CT scanner (11). However, the results were limited in precision and were not considered clinically useful at that time.

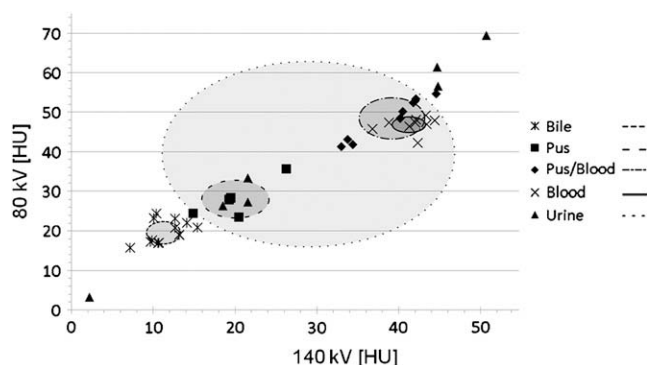


**Figure 3.** Attenuation ranges of the different sample types at 80 and 140 kV. The shaded ellipses were added as a visual aid. They are surrounded by different linings indicating the corresponding fluid. The center points represent the arithmetic mean of the different fluids computed tomographic values, whereas the axis lengths indicate the standard deviation for the corresponding sample. Bile and pus are distinguishable from blood and the blood/pus mixture. The attenuation values of the other samples are indistinguishable due to overlaps.

For spectral CT imaging the difference between the x-ray spectra should be as pronounced as possible. In clinical computed tomography, there are some limits to the x-ray spectra. Most clinical CT scanners cover the range from 80 to 140 kV. Lower tube voltages are not available, as there is normally not enough tube power to provide enough quanta for achieving acceptable noise levels. Applying the ex vivo scan protocol as previously described to in vivo studies will result in a clinically unacceptable radiation exposure. This is of particular interest, because for patients examinations, even higher tube current-time products might be needed to correct for tissue attenuation. Moreover, the tube current-time products need to be adjusted to achieve similar noise levels. High-dose image acquisition is not a problem as long as the scan range is limited to a single slice. For volumetric data acquisition, however, strategies for keeping the radiation

**Table 1**  
**Summary of the Attenuation Values at Different Tube Voltages, Mass Densities, and Effective Atomic Numbers as Computed using the  $\rho Z$ -algorithm. Except for Pus and Bile, Attenuation Values are Widely Overlapping, Limiting Fluid Differentiation**

	80 kV [HU]	140 kV [HU]	Mass Density [ $\rho$ ; g/cm <sup>3</sup> ]	Eff. Atomic Number [ $Z_{eff}$ ]
Blood (n = 9)	46.8 ± 2.0 (42.2–49.2)	41.6 ± 2.4 (36.8–44.4)	1.038 ± 0.005 (1.031–1.045)	7.577 ± 0.020 (7.560–7.610)
Blood + Pus (n = 9)	48.7 ± 5.3 (41.3–54.6)	39.2 ± 4.3 (33.0–44.6)	1.027 ± 0.005 (1.020–1.035)	7.636 ± 0.043 (7.580–7.700)
Pus (n = 5)	27.9 ± 4.8 (23.5–35.6)	20.1 ± 4.1 (14.9–26.3)	1.011 ± 0.003 (1.008–1.014)	7.676 ± 0.041 (7.630–7.730)
Bile (n = 13)	20.0 ± 3.1 (15.8–24.4)	11.9 ± 2.7 (7.2–15.4)	1.005 ± 0.007 (0.990–1.014)	7.625 ± 0.028 (7.600–7.690)
Urine (n = 7)	39.7 ± 3.6 (3.2–69.4)	29.2 ± 17.8 (2.2–50.7)	1.022 ± 0.011 (1.003–1.034)	7.744 ± 0.149 (7.460–7.890)

Data are given as Mean ± Standard Deviation. Values in Brackets Indicate Minimum and Maximum.

exposure in acceptable ranges, while ensuring a sufficient image quality, have to be sought. Another strategy for improving data quality is to optimize the separation of the different x-ray spectra. For this purpose different Ti filter settings of the x-ray tube were used, which further shift the 140 kV spectrum to higher energies compared with the 80 kV spectrum (Fig 1).

In retrospect, there were several reasons for the limited clinical acceptance of dual-energy imaging at that time. Physical model functions as well as empirical material basis functions only approximate representations of the actual body attenuation function. The precision of both methods to reconstruct elemental attenuation spectra in the clinically relevant range from  $Z_{eff} = 1$  to  $Z_{eff} = 20$  creates systematical errors in the range of around  $\Delta Z_{eff} = 0.6$  to  $\Delta Z_{eff} = 0.8$  in the atomic number reconstruction (12). Moreover, the detector response function  $D(E)$  is not included in the original description (4,5). Consequently, CT projections through a mixture of materials will systematically over- or underestimate the governing physical material parameter. Considering the reported experimental data, an accuracy of 0.1 to 0.2 is required for  $Z_{eff}$  to permit reliable fluid and soft tissue identification (12). Thus, material decomposition is of only limited value for tissue characterization.

From experimental data in anorganic material it is known that  $\rho Z$  projected data achieve a very high precision with  $\Delta Z = 0.1$  and  $\Delta \rho = 0.002$  g/cm<sup>3</sup> (6). The presented data show that a similar precision can be obtained from organic materials. Comparing simple attenuation data at 80 and 140 HU with the  $\rho Z$  projected data blood, mixture of blood and pus, as well as pus samples can now be differentiated, providing a diagnostic advantage compared to solely attenuation based assessment of dual-energy data. This finding illustrates a general feature of the  $\rho Z$ -projection, the ability to distinguish between an attenuation increase by atomic number or mass density, i.e., chemical or morphologic changes. For instance, two samples with effective densities  $\rho_1, \rho_2$ , with  $\rho_1 > \rho_2$  and atomic numbers  $Z_1, Z_2$ , with  $Z_1 < Z_2$ , can actually have the same attenuation  $\mu$ , but will differ in the measured  $\rho$  and  $Z_{eff}$ . In these cases, the  $\rho Z$ -projection is a valuable tool for increasing contrasts.

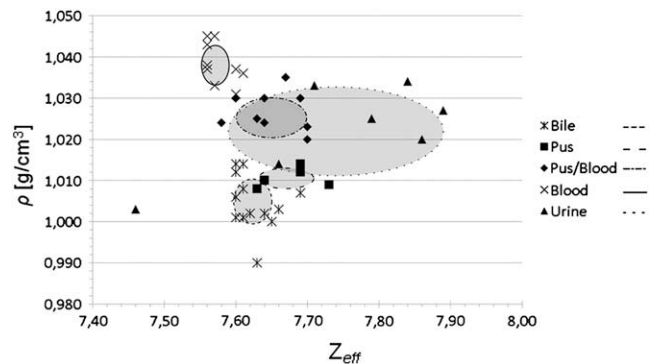


**Figure 4.** The  $\rho Z$  diagram shows a clustering of the samples. The center points of the shaded ellipses represent the arithmetic means of  $\rho$  and  $Z_{eff}$  values of the different samples, whereas the axis lengths indicate the standard deviation for the corresponding sample. Pus and blood can be clearly distinguished, while bile and pus partly overlap. The mixture of blood and pus has intermediate values, but it can be differentiated from the blood samples. The latter is not possible using the attenuation values alone.

Nevertheless, this technique does not solve all of the diagnostic problems in fluid differentiation. For instance, urine was not distinguishable as there was a very broad standard deviation in the attenuation as well as in the  $\rho Z$  images, making urine indistinguishable from other substances. In some patients, CT values of up to 50.7 HU were measured at 140 kV in urine, which is uncommon in clinical computed tomography. This finding was observed in dehydrated patients only. It is due to the changing concentration of electrolytes and uric acid in the urine depending on the state of hydration of the patient, i.e., this effect is due to probe variation. In contrast, blood as a more stable body fluid, with much less deviations from its average composition, was easily distinguishable from other substances. The measured  $\rho$  and  $Z_{eff}$  values for blood can be compared to experimental data from the ICRU 46 report (13). It reports an expected density of  $\rho_{blood} = 1.060$  g/cm<sup>3</sup>. The CT measured density differs by  $\Delta \rho = -0.022$  g/cm<sup>3</sup>. This could be due to different stages of aging for the measured blood samples because clotting and oxidation change the chemical composition and density distribution.

Table 2

The Means of the Five Categories of Fluids were Compared for the Attenuation Values at 80 and 140 kV, Mass Density, and Effective Atomic Number with *t*-tests. Applying the  $\rho Z$  Projection Method, Blood becomes Distinguishable from Mixtures of Blood and Pus with  $\rho$  and  $Z_{eff}$  being Significantly Different for each Fluid. For the other Categories of Fluids, there are No Major Differences Comparing the Attenuation Values with the Results of the  $\rho Z$  Projection Method

	Parameter	Blood + Pus	Pus	Bile	Urine
Blood	80 kV	$P = .3293$	$P < .0001$	$P < .0001$	$P = .3795$
	140 kV	$P = .1631$	$P < .0001$	$P < .0001$	$P = .0557$
	$\rho$	$P = .0003$	$P < .0001$	$P < .0001$	$P = .0016$
	$Z_{eff}$	$P = .0018$	$P < .0001$	$P = .0003$	$P = .0047$
Blood + Pus	80 kV	-	$P < .0001$	$P < .0001$	$P = .2820$
	140 kV	-	$P < .0001$	$P < .0001$	$P = .1232$
	$\rho$	-	$P < .0001$	$P < .0001$	$P = .2426$
	$Z_{eff}$	-	$P = .1161$	$P = .4743$	$P = .0559$
Pus	80 kV	-	-	$P = .0007$	$P = .3023$
	140 kV	-	-	$P < .0001$	$P = .2939$
	$\rho$	-	-	$P = .0866$	$P = .0569$
	$Z_{eff}$	-	-	$P = .0076$	$P = .3494$
Bile	80 kV	-	-	-	$P = .0072$
	140 kV	-	-	-	$P = .0025$
	$\rho$	-	-	-	$P = .0005$
	$Z_{eff}$	-	-	-	$P = .0106$

Quantitative CT methods suffer some well-known limitations. These include quantum noise, scattered radiation, and beam hardening. Although scatter and beam hardening have different origins, the affected portions of an image are similar. Projections through bone or metal implants are usually at the same time affected by an increased scattering component and the CT approximation error attributed to beam hardening. This means that without a correction of these effects, the affected image regions are typically not accessible to quantitative or spectral CT methods. However, for most soft tissue regions in the abdomen or chest, the impact of beam hardening and scattering on CT values is low. Nevertheless, these disturbances need to be considered during data acquisition. The use of a high tube current-time product reduces image noise and beam hardening by minimizing the photon starvation effect. Sequential image acquisition without table movement was used to avoid motion and co-registration errors.

Beyond these general problems with quantitative CT imaging, there are some limitations that are specifically related to this study. First, all probes were measured outside the human body, reducing the attenuation of the surrounding body. Using these near ideal conditions, there are less artifacts compared to an in vivo situation. Correspondingly, there were no visible artifacts. Nevertheless, the regions-of-interest were placed in the center of the probes to avoid so-called edge overshoots. Second, all body fluids are not stable outside the human body and the measured attenuation values may differ from in vivo measurements. To minimize this effect, all samples were scanned as soon as possible after the

puncture, generally within less than 10 minutes. Third, all data were acquired with an outdated 4-slice CT scanner. As only ex vivo measurements were performed, this should not affect results. Finally, the sharp convolution kernel that was used for image reconstruction increases image noise. It was thought to be useful as it improves spatial resolution, which was needed because of the small sample tubes. As the maximum tube current-time product was used for image acquisition, the image noise was kept in acceptable ranges. In a clinical setting, however, the use of a standard medium smooth convolution kernel is likely to further improve accuracy.

With introduction of dual-source computed tomography in clinical routine new efforts for establishing material sensitive imaging have been made (14–16). This technique allows for simultaneous data acquisition with two different tube voltages, omitting the need for two separate data acquisitions as has been done in this study. Thereby, dual-source computed tomography overcomes some of the previous problems of dual-energy imaging. Particularly, motion artifacts are no longer a problem, as both image sets at different energy settings are acquired simultaneously. This is a fundamental for establishing dual-energy computed tomography in clinical routine. Moreover, the availability of two independent tube-detector systems provides sufficient power reserves to acquire high quality image data at two different energy settings without the need for switching the tube voltage, as it has been done in an early implementation of dual-energy computed tomography (11). The  $\rho Z$ -projection method gives way to a truly quantitative assessment of

dual-energy CT images. This does not only permit the characterization of fluid collections, but also allows for a quantitative analysis of tissue composition. Quantitative information on mass density may also help to improve radiation therapy planning. The growing number of CT scanners with dedicated dual-energy scan protocols, will result in an increased clinical utilization of dual-energy CT imaging in the near future.

**CONCLUSION**

In conclusion, the  $\rho Z$ -projection method is suited to quantitatively assess mass density and effective atomic number of ex vivo body fluid samples. It provides valuable information on chemical and physical characteristics of organic substances and might be useful for the characterization of otherwise undetermined fluid collections. As the  $\rho Z$ -projection method works with unenhanced computed tomography, it is particularly suited for patients who may not receive iodinated contrast agents. Our preliminary results warrant further investigations in an in vivo setting.

**REFERENCES**

1. Filly RA, Sommer FG, Minton MJ. Characterization of biological fluids by ultrasound and computed tomography. *Radiology* 1980; 134:167-171.
2. Gupta S, Seith A, Sud K, et al. CT in the evaluation of complicated autosomal dominant polycystic kidney disease. *Acta Radiol* 2000; 41: 280-284.
3. Nandalur KR, Hardie AH, Bollampally SR, et al. Accuracy of computed tomography attenuation values in the characterization of pleural fluid: an ROC study. *Acad Radiol* 2005; 12:987-991.
4. Alvarez RE, Macovski A. Energy-selective reconstructions in X-ray computerized tomography. *Phys Med Biol* 1976; 21:733-744.
5. Macovski A, Alvarez RE, Chan JL, et al. Energy dependent reconstruction in X-ray computerized tomography. *Comput Biol Med* 1976; 6:325-336.
6. Heismann BJ, Leppert J, Stierstorfer K. Density and atomic number measurements with spectral x-ray attenuation method. *J Appl Phys* 2003; 94:2073-2079.
7. Stonestrom JP, Alvarez RE, Macovski A. A framework for spectral artifact corrections in x-ray CT. *IEEE Trans Biomed Eng* 1981; 28:128-141.
8. Weaver JB, Huddleston AL. Attenuation coefficients of body tissues using principal-components analysis. *Med Phys* 1985; 12:40-45.
9. Vetter JR, Holden JE. Correction for scattered radiation and other background signals in dual-energy computed tomography material thickness measurements. *Med Phys* 1988; 15:726-731.
10. Avrin DE, Macovski A, Zatz LE. Clinical application of Compton and photo-electric reconstruction in computed tomography: preliminary results. *Invest Radiol* 1978; 13:217-222.
11. Kalender WA, Perman WH, Vetter JR, et al. Evaluation of a prototype dual-energy computed tomographic apparatus. I. Phantom studies. *Med Phys* 1986; 13:334-339.
12. Heismann BJ. Atomic number measurement precision of spectral decomposition methods for CT. *IEEE Nuclear Science Symposium Conference Record* 2005; 5:2741-2742.
13. International Commission on Radiation Units and Measurements (ICRU). Photon, electron, proton and neutron interaction data for body tissues (Report 46). Bethesda, MD: ICRU, 1992.
14. Johnson TR, Krauss B, Sedlmair M, et al. Material differentiation by dual energy CT: initial experience. *Eur Radiol* 2007; 17:1510-1517.
15. Pontana F, Faivre JB, Remy-Jardin M, et al. Lung perfusion with dual-energy multidetector-row CT (MDCT): feasibility for the evaluation of

- acute pulmonary embolism in 117 consecutive patients. *Acad Radiol* 2008; 15:1494-1504.
16. Primak AN, Fletcher JG, Vrtiska TJ, et al. Noninvasive differentiation of uric acid versus non-uric acid kidney stones using dual-energy CT. *Acad Radiol* 2007; 14:1441-1447.
17. Perkins ST, Cullen DE, Chen MH, et al. Tables and graphs of atomic subshell and relaxation data derived from the LLNL evaluated atomic data library (EADL), Z = 1-100. Lawrence Livermore National Laboratory Report UCRL-50400, Vol. 30. Livermore, CA, 1991.
18. Cullen DE, Chen MH, Hubbell JH, et al. Tables and graphs of photon-interaction cross-sections from 10 eV to 100 GeV derived from the LLNL evaluated photon data library. Lawrence Livermore National Laboratory Report UCRL-50400, Vol. 6. Livermore, CA, 1989.

**APPENDIX**

This appendix summarizes essential basics of the  $\rho Z$ -projection; details of the algorithm were described by Heismann et al (6). Based on reconstructed CT images in Hounsfield units,  $H_1(\vec{r}), H_2(\vec{r})$ , the  $\rho Z$ -projection inverts a dual-energy CT measurement into a mass density  $\rho$  and an effective atomic number  $Z_{\text{eff}}$ . The basic idea is to use the attenuation functions  $\kappa(E, \rho, Z)$  of the chemical elements as basis functions (6).

Consider measuring two attenuation factors  $\mu_1, \mu_2$  with two different spectral weightings  $w_1, w_2$ . Using the standard Radon approximation, the measurements are described by

$$\begin{pmatrix} \mu_1 \\ \mu_2 \end{pmatrix} = \rho \cdot \begin{pmatrix} \int w_1(E) \left(\frac{\kappa}{\rho}\right)(E, Z) dE \\ \int w_2(E) \left(\frac{\kappa}{\rho}\right)(E, Z) dE \end{pmatrix} = \rho \begin{pmatrix} f_1(Z) \\ f_2(Z) \end{pmatrix}. \quad (1)$$

Here the spectral attenuation coefficient ( $\kappa/\rho$ ) is factorized into the mass density  $\rho$  and the specific spectral attenuation function ( $\kappa/\rho$ )(E). Note that the left side of (Eqn 1) contains the measured values

$$\mu_i = \left(1 + \frac{H_i}{1000}\right) \mu_{H_2O} \quad (2)$$

and the right side can be calculated for the known spectral weighting functions  $w_i(E)$  and elemental atomic basis functions ( $\kappa/\rho$ )(E).

The central idea of the  $\rho Z$ -projection is to invert (Eqn 1) for the density and atomic number:

$$\begin{pmatrix} \mu_1(\rho, Z) \\ \mu_2(\rho, Z) \end{pmatrix} \rightarrow \begin{pmatrix} \rho(\mu_1, \mu_2) \\ Z(\mu_1, \mu_2) \end{pmatrix}. \quad (3)$$

As the numerical solution

$$\begin{aligned} Z &= F^{-1} \begin{pmatrix} \mu_1 \\ \mu_2 \end{pmatrix}, \\ \rho &= \frac{\mu_1}{f_1(Z)} = \frac{\mu_1}{f_1 \left( F^{-1} \begin{pmatrix} \mu_1 \\ \mu_2 \end{pmatrix} \right)} \end{aligned} \quad (4a, b)$$

is obtained with

$$\begin{aligned} f_i(Z) &= \int w_i(E) \left(\frac{\kappa}{\rho}\right)(E, Z) dE, \\ F(Z) &= \frac{f_1(Z)}{f_2(Z)}. \end{aligned} \quad (5a, b)$$

The functions  $f_1(Z)$ ,  $f_2(Z)$  and  $F(Z)$  can be calculated prior to the measurement with the known spectral weighting functions  $w_i(E)$  and tabulated  $(\kappa/\rho)(E, Z)$  from experimental data by, e.g., Perkins et al (17) and Cullen et al (18). Equations (3a, b) directly transform two measured images into  $\rho$  and  $Z$  images. For medical computed tomography we can generally expect  $Z_{\text{eff}}$  to be lying in the interval [1... 20] and  $\rho$  in the interval [0... 2] g/cm<sup>3</sup>.

Generally, Equation (4a) yields non-integer  $Z$  values. For a compound attenuator of  $n$  elements with individual partial densities  $\rho_k$  and atomic numbers  $Z_k$  the following measurement will be made:

$$\mu = \sum_{k=1}^n \rho_k \int w(E) \left(\frac{\kappa}{\rho}\right)(E, Z_k) dE. \quad (6)$$

For a known stoichiometric composition of a compound material the associated  $Z_{\text{eff}}$  can be calculated.

Two measurements ( $\mu_1, \mu_2$ ) can be inverted according to (3) to a fractured  $Z$ . It is intrinsically defined by the system weighting  $w(E)$  and the modeling of the spectral attenuation coefficient  $(\kappa/\rho)(E, Z)$  for non-integer  $Z$ . A linear composition is a valid choice for this purpose, defining a virtual attenuator, e.g.,  $Z = 7.4$  by summing 40% of a  $Z = 7$  (nitrogen) spectrum and 60% of a  $Z = 8$  (oxygen) spectrum. The effective  $Z$  obtained by the  $\rho Z$ -projection identifies the corresponding virtual absorber and the effective density according to (Eqn 1).

The model mismatch error increases with the distance to the basis functions. In the case of the  $\rho Z$ -projection a basis function is given for each integer  $Z$ , significantly decreasing the model mismatch error. It was shown for chemical solutions of known density and composition that the precision of reconstruction is about 0.1 for  $Z_{\text{eff}}$  and 0.020 g/cm<sup>3</sup> for  $\rho$  (Eqn 6).